ON THE COMPETITION AMONG MAGNETIC AND HYDRODYNAMIC INSTABILITIES IN MAGNETIZED SHEARED PLASMA FLOWS

F. Pegoraro, M. Faganello, F. Califano, A. Tenerani

Physics Department   University of Pisa   pegoraro@df.unipi.it

Overview

The **Kelvin-Helmholtz**, the **Rayleigh-Taylor** and the **Magnetic Reconnection** instabilities play a fundamental role in the nonlinear dynamics of a magnetized, spatially inhomogeneous plasma

They can be driven directly or indirectly, i.e., as "secondary instabilities", by inhomogeneities of the plasma fluid velocity, of the density (or pressure) it the plasma is subject to a (centrifugal) acceleration and, in the case of magnetic reconnection, by inhomogeneities of the plasma currents.

These instabilities do not occur separately and the time evolution of the system as a whole depends on their nonlinear interaction.

This complex interaction is governed by the time scales of the different processes at play.

These processes involve both large spatial scales from which e.g., the initial drive of the primary Kelvin-Helmholtz instability originates, and small spatial scales generated in the nonlinear evolution of the primary instability, where e.g., magnetic field line reconnection can occur.

The timing between these instabilities will determine the structure of the final configuration that the system can reach.

The structural differences between the possible final states can in principle be used as a diagnostic tool in order to determine experimentally how fast the different instabilities evolve.

In this presentation I will review recent results that have been obtained by means of two-dimensional, two-fluid numerical simulations of the interplay between large scale and small scale dynamics in the framework of the nonlinear evolution of a magnetized plasma configuration with a velocity shear field.

Faganello M *et al.* 2008a Phys. Rev. Lett. **100** 015001.
Faganello M *et al.* 2008b Phys. Rev. Lett. **101** 105001.
Faganello M *et al.* 2008c Phys. Rev. Lett. **101** 175003.
Pegoraro F *et al.* 2008 Journal Physics Conference, Series **133**, paper 012024.
Califano F *et al.* 2009 Nonlin. Processes Geophys., **16** 1 (2009).
Faganello M *et al.* 2009 New Journal Phys, **11** 063008.
Tenerani A *et al.* 2010 submitted to Plasma Physics and Controlled Fusion.

The observational problem that can be addressed in this way concerns the mixing that occurs between the solar wind plasma and the magnetospheric plasma and its development as the solar wind streams downward past the Earth at the flank of the Earth's magnetosphere at low latitudes.

The Kelvin-Helmholtz instability has been shown[1] to play a crucial role in the interaction between the solar wind and the Earth's magnetosphere and to provide a mechanism by which the solar wind can enter the Earth's magnetosphere (mixing of the solar wind and of the magnetospheric plasmas)[2]

In particular, the KH instability can grow along the flank magnetopause at low latitude, where a velocity shear exists and where the nearly perpendicular magnetic field does not inhibit the development of the instability[3].

Several observations support this explanation and show that the physical quantities observed along the flank magnetopause at low latitude are compatible with a Kelvin-Helmholtz vortex[4].

---

[1]H. Hasegawa *et al.*, Nature **430**, 755 (2004).

[2]D. G. Mitchell, J. Geophys. Res. **92**, 7394 (1987); H. Hasegawa *et al.*, Geophys. Res.Lett. **431**, L06802 (2004)

[3]A. Miura, Phys. Rev. Lett. **16**, 779 (1982); J.U. Brackbill *et al.*, Phys. Rev. Lett.**86**, 2329 (2001); C. Hashimoto *et al.*, Adv. Space. Res **37**, 527 (2006)

[4]H. Hasegawa *et al.*, Nature **430**, 755 (2004); D.H. Fairfield *et al.*, J. Geophys. Res. **105**, 21159 (2000); A. Otto *et al.*, J. Geophys. Res. **105**, 21175 (2000).
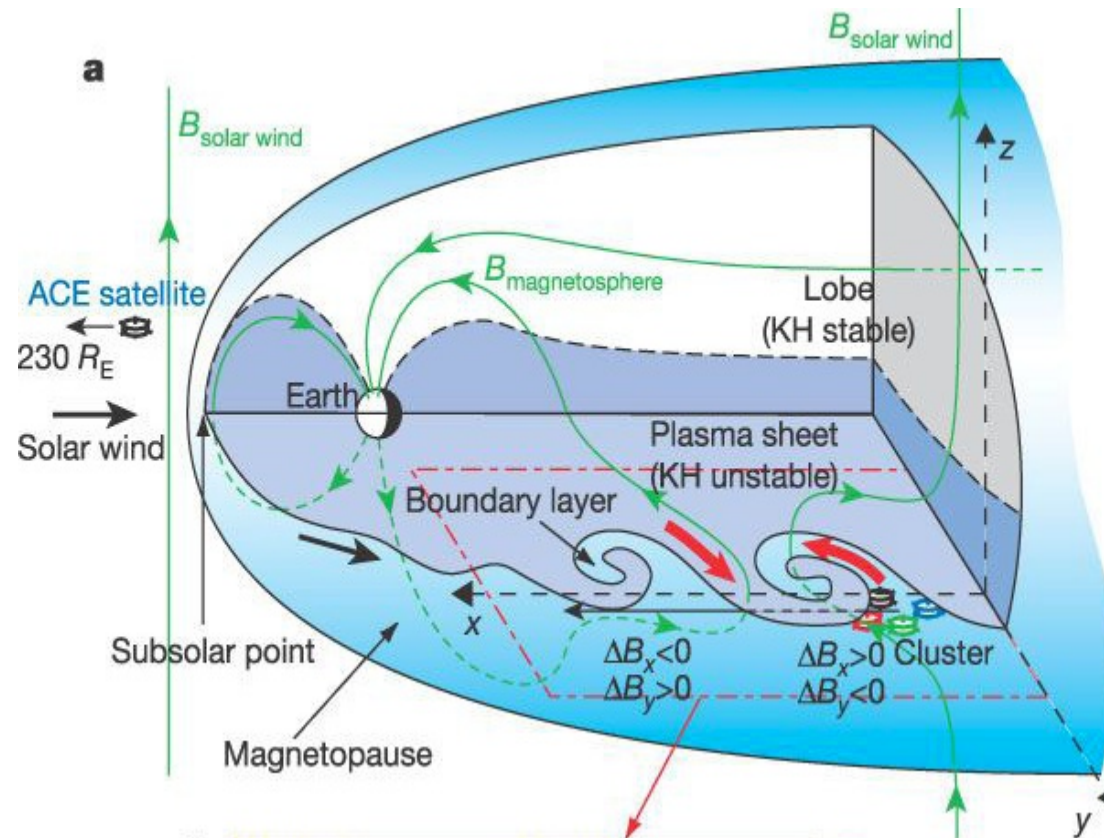
Figure 1: Solar wind interaction with the Earth magnetosphere, from H. Hasegawa *et al.*, Nature **430**, 755 (2004).

Plasma description and relevant control parameters

The investigation of the nonlinear plasma behaviour in regimes that can shed light e.g., on the dynamics of the solar wind interaction with the Earth's magnetosphere would require a fully kinetic plasma treatment, three-dimensional in coordinate space and three-dimensional in velocity space.

At present such an approach is not feasible, even numerically, because global (large scale) and local (small scale) effects are both to be accounted for, as they affect each other and thus their evolution cannot be separated.

Nevertheless relevant information can be obtained by performing fully nonlinear numerical simulations in a simplified two dimensional geometry and by adopting a two fluid plasma description.

Within this description large scale hydrodynamic and magnetohydrodynamic effects can be treated together with small scale effects.

Small scale effects are related to the decoupling between electrons and ions at the ion inertial skin length scale $d_i \equiv c/\omega_{pi}$ (Hall term in Ohm' s law) and the decoupling between the magnetic field and the electron fluid at the electron inertial skin length scale $d_e \equiv c/\omega_{pe}$ (that allows for magnetic reconnection to occur even in the absence of dissipation).

Such a description makes it possible to explore different regimes by changing in the simulations the values of a set of control parameters that characterize the properties of the initial configuration.

In the following I will consider an equilibrium given by a spatially inhomogeneous magnetized plasma with an initial velocity field in the y-direction, sheared in the x-direction:

$$U_y(x) = \frac{\Delta U}{2} \tanh\left(\frac{x - \frac{L_x}{2}}{L_{eq}}\right),$$

$$n(x) = n_0 \left[\left(1 - \frac{\Delta n}{2}\right) + \Delta n \tanh\left(\frac{x - \frac{L_x}{2}}{L_{eq}}\right)\right],$$

$$P_{e/i}(x) = n(x)T_{e/i}, \quad B_z = B_z(x), \quad B_y = B_{y0},$$

with n_0, $P_{0e/i}$ the values at the right boundary of the simulation box of the electron and ion density and pressure, $B_0 = B_z(0)$ the corresponding value of the magnetic field component along z and $T_{e/i}$ the uniform electron and ion temperature.
The total pressure is initially uniform.

Control Parameters (at fixed and equal electron and ion temperatures)

ΔU controls the velocity inhomogeneity i.e. the onset of the Kelvin Helmholtz (KH) instability,

Δn controls the density inhomogeneity, i.e. the onset of the Rayleigh Taylor (RT) instability in the presence of a centrifugal acceleration,

L_{eq} is the equilibrium velocity shear length,[5]

B_{y0} controls the stabilizing effect on the KH instability of the field line tension and, when sheared by the plasma motion, can give rise to magnetic reconnection,

B_z ensures pressure balance, controls plasma compressibility and the role of the Hall term.

---

[5]it determines the wave length of the fastest growing mode of the KH vortices.
For simplicity it is taken equal to the density inhomogeneity scalelength.

The plasma β parameter and the sonic and Alfvènic Mach numbers can be expressed in terms of these parameters.

In the following the control parameters of the equilibrium configuration are chosen in such a way that the equilibrium is KH unstable, but such that it is RT stable (there is no gravity or, initially, a centrifugal acceleration) and magnetic reconnection cannot occur (in-plane magnetic field initially uniform).

The nonlinear evolution of the KH instability changes this situation and allows for both RT and reconnection to occur.

How RT and reconnection compete and, in particular, how they affect the process of vortex merging that is the fundamental process in the nonlinear evolution of the KH instability is the main aim of this presentation.
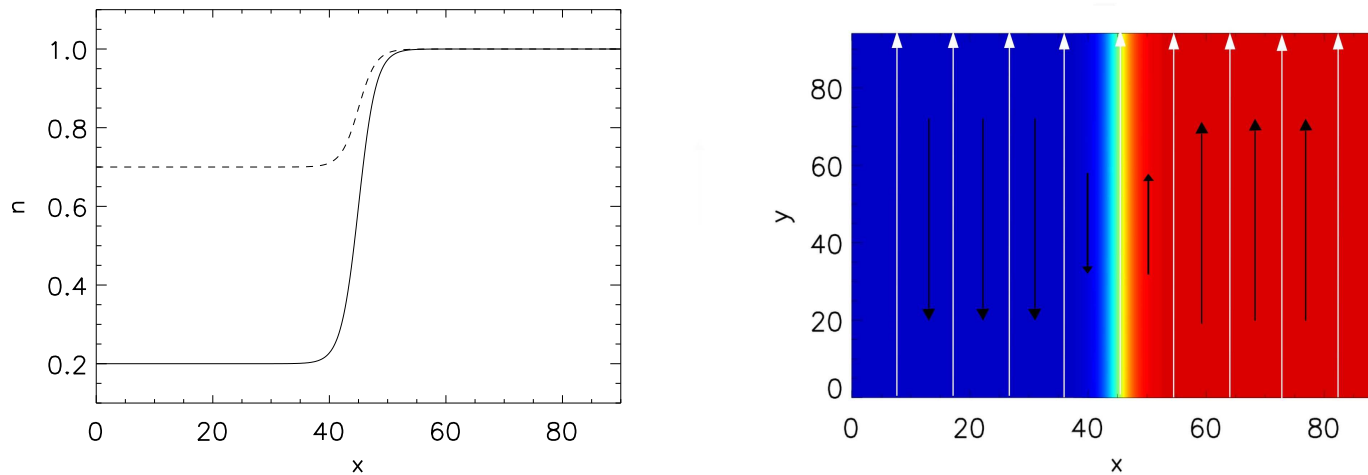
Primary and secondary instabilities

Figure 2: Left frame: initial density profile versus x for $\Delta n = 0.3$ (dashed line) and for $\Delta n = 0.8$ (solid line). Right frame: shaded isocontours of the plasma density. The white (black) arrows represent the in-plane magnetic (velocity) field lines.

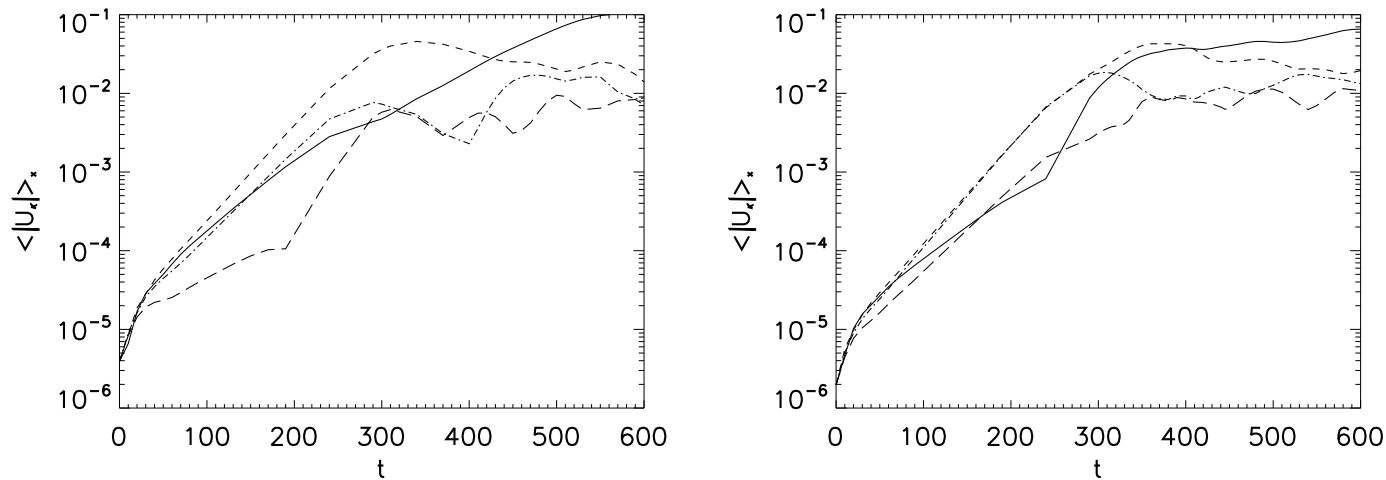I will use the shaded isocontours of the density in order to visualize the plasma evolution.

Figure 3: Time evolution of the Fourier amplitudes $m = 1$ (solid line), $m = 2$ (short dashed line), $m = 3$ (dot-dashed line) and $m = 4$ (long dashed line) of the x-averaged velocity field along y for $\Delta n = 0.3$ (left frame) and for $\Delta n = 0.8$ (right frame).

Examining the early stage (from $t = 0$ up to nearly $t = 150$) of the mode evolution shown in Fig. 3, we obtain the value of m corresponding to the fastest growing mode (FGM) of the KH instability and its growth rate.

For $\Delta n = 0.3$ the FGM mode corresponds to $m = 2$ and has a growth rate $\gamma_2 \sim 0.028$, while for $\Delta n = 0.8$ the modes corresponding to $m = 2$ and $m = 3$ have nearly the same growth rates $\gamma_2 \sim 0.029$ and $\gamma_3 \sim 0.030$.

We see that the density jump does not influence the linear growth rate of the FGM of the KH instability significantly which in this phase develops essentially on the same time scale, almost independently of the value of Δn.

At later times, $t > 300$, the fastest growing modes develop into fully rolled-up vortices, as shown in Fig. 4. For $\Delta n = 0.3$ we thus observe the growth of two vortices (see Fig. 4 first row, left frame) and for $\Delta n = 0.8$ the growth of three unequal vortices (see Fig. 4 second row, left frame), consistently with the FGM wave numbers calculated in the linear stage.
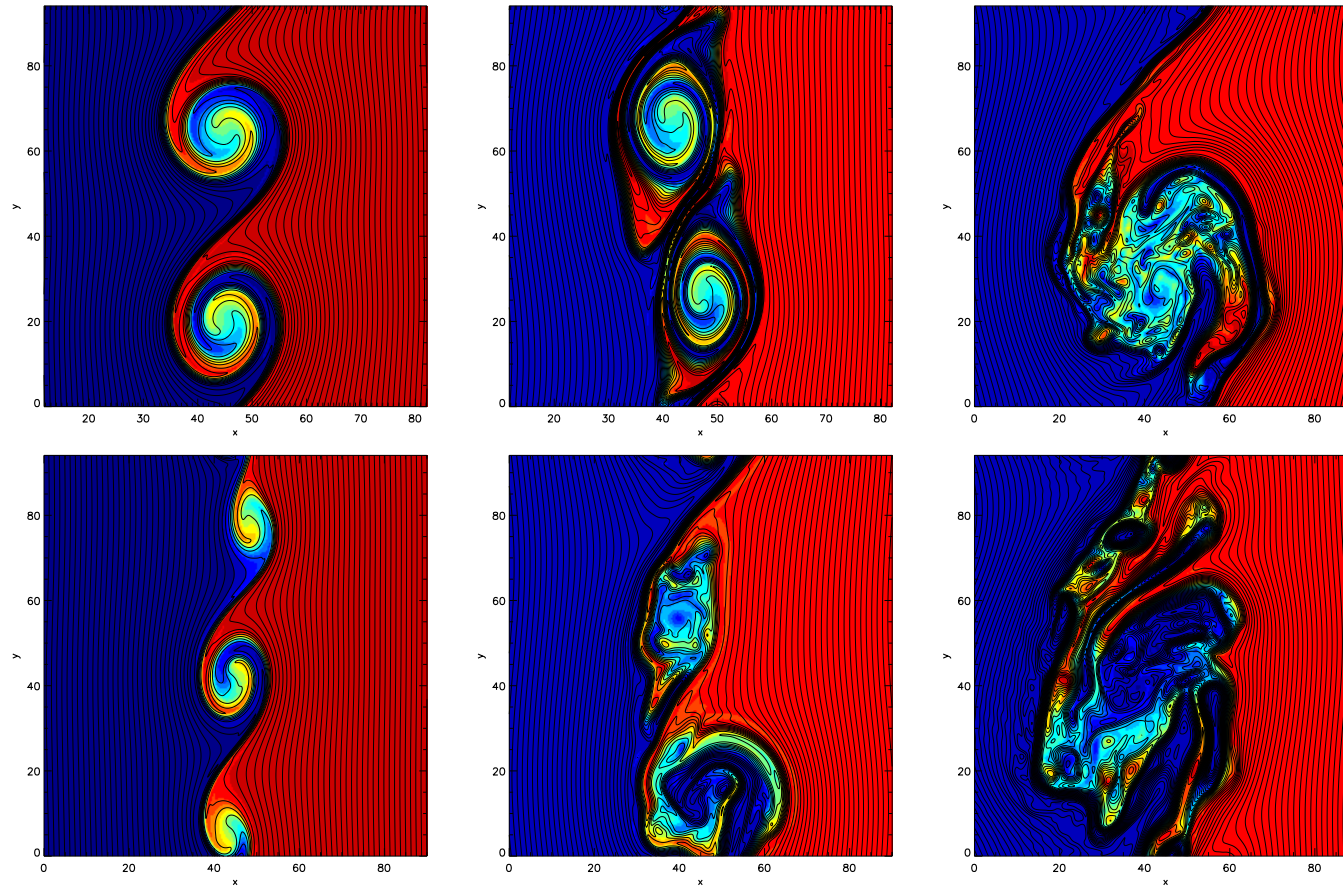
Figure 4: Time evolution of the KH vortices for $\Delta n = 0.3$ (first row, at $t = 340$, 437.5, 590 from left to right) and for $\Delta n = 0.8$ (second row, at $t = 310$, 405, 640).

Further in time, the system develops two kind of processes: the pairing of the vortices and the development of secondary instabilities inside each vortex due to the rolling-up of the plasma.

We can see in Fig. 4 that the vortices tend to merge together during their non linear evolution and to generate a single large-scale vortex, following the typical 2-D hydrodynamical[6]and MHD[7] pairing process. In addition, as shown in more detail in the following section, the rolling up of the vortices is able to create favourable conditions for the development of secondary RT and KH instabilities inside each vortex. In fact, the density and velocity differences between the vortex arms, combined with the rotational motion of the vortex, allow the RT and KH instabilities to grow along the vortex arms.

---

[6]C.D. Winant *et al.*, J. Fluid Mech. **63**, 237 (1974).   F.K. Browand *et al.*, J. Fluid Mech. **76**, 127 (1976).

[7]A. Miura, Phys. Plasmas **4**, 2871 (1997). A. Miura, J. Geophys. Res. **104**, 395 (1999).   A. Miura, Geophys. Res. Lett. **26**, 409 (1999).

In such a complex picture reconnection of the field lines of the in-plane magnetic field also take place.

Because of the frozen-in constraint which is satisfied during the formation of the vortex, the magnetic field is carried and stretched by the plasma motion, so that the in-plane magnetic field develops inversion regions where field lines can reconnect.

When (before or during the pairing process) and where (inside the vortex arms or between the pairing vortices) magnetic reconnection takes places depends on the competition between the vortex pairing and the development of the secondary RT instability.

The competition between the pairing process and the hydrodynamic secondary instabilities plays a crucial role in determining the final state of the system.

For $\Delta n = 0.3$ the secondary KH and RT instabilities induced inside the vortices are weak and the evolution of the primary KH instability leads to a typical pairing process (see Fig. 4, first row). The two vortices begin to merge following the pairing process (central frame) until they form a single vortex (right frame).

For $\Delta n = 0.8$ the system of three vortices also follows the pairing process but at the same time the perturbations growing inside the vortices tend to destroy them. The two vortices located at the (periodic) boundaries along the y-direction of the simulation box merge in one vortex while the RT instability strongly perturbs the structure of the vortices (central frame).

Despite these growing perturbations, no complete disruption of the vortices takes place because of the partial stabilizing effect of the in-plane magnetic field, as will be discussed later, and a configuration characterized by a single structure is achieved, strongly perturbed by the RT instability which creates macroscopic sub-structures inside the main structure (right frame).

Onset of secondary "hydrodynamic" instabilities

I will mainly refer to the results obtained in the case with $\Delta n = 0.8$

The development of the KH instability leads to the formation of fully rolled up vortices. During this process the red and the blue portions of the initial plasma configuration envelop one another forming regions with alternating density values. The plasma in the vortices is set into an approximately circular motion and the associated centrifugal force acts as an effective gravity.
The simultaneous presence of regions with different densities and a "gravitational" acceleration generates RT unstable configurations inside each vortex.

As the primary KH instability grows, the lesser dense plasma acquires a higher velocity than the denser plasma.
In Fig. 5 the profiles of the density (blue line) and of the tangential velocity (black line) taken along the line passing through the center of one of the vortices are shown; the left frame refers to $\Delta n = 0.8$ and the right frame to $\Delta n = 0.3$.
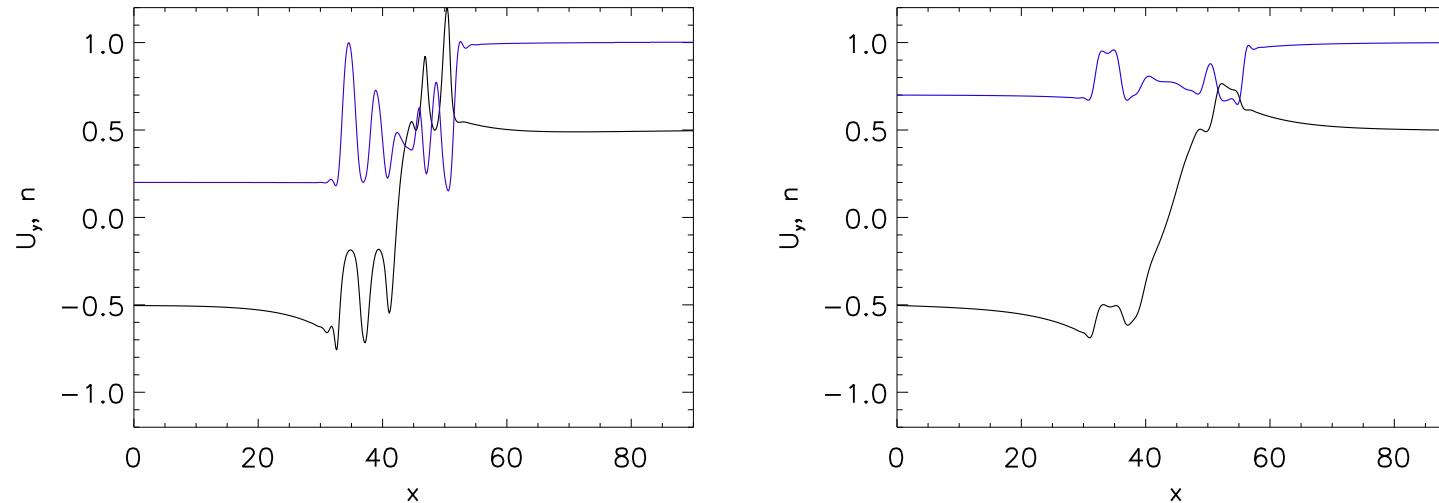
Figure 5: Left frame: profiles of the tangential velocity $U_y(x)$ (black line) and density $n(x)$ (blue line) at time $t = 350$ along the line $y = 47$ passing through the vortex center for $\Delta n = 0.8$. Right frame: profiles of the tangential velocity $U_y(x)$ (black line) and density $n(x)$ (blue line) at time $t = 370$ along the line $y = 64$ passing through the vortex center for $\Delta n = 0.3$. Note that $U_y(x)$ changes sign at the vortex center.

These plots show that the velocity in the lower density regions is in absolute value larger than in the denser regions. This asymmetry causes the formation of velocity shears inside the vortices where the plasma can become unstable to a secondary KH instability.

By comparing the two velocity plots shown in Fig. 5 it is evident that not only the density difference but also the velocity shears are stronger when the density jump is greater. Therefore we can expect the hydrodynamic secondary instabilities to be weaker for $\Delta n = 0.3$ than for $\Delta n = 0.8$. In fact from Fig. 6 which shows one of the vortices at $t = 345$, $t = 369$ and $t = 405$ for $\Delta n = 0.8$, we can see a growing perturbation inside the vortex with a typical wave length of $\lambda \sim 5 - 10$, whereas in the case $\Delta n = 0.3$ no strong perturbations develop (not shown).
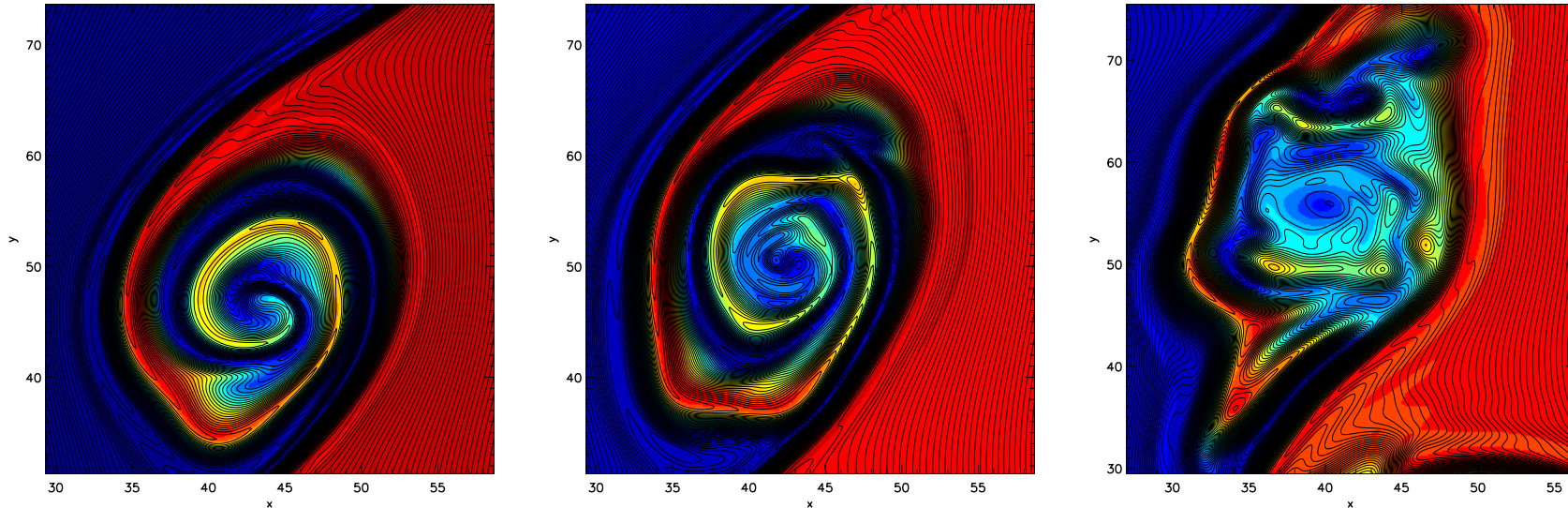
Figure 6: Vortex development and rolling up for $\Delta n = 0.8$: detailed evolution of the central vortex at $t = 345,\ 369,\ 405$.

Note that the in-plane magnetic field has a stabilizing effect and that completely inhibits perturbations with wave length $\lambda < 1$.

Rayleigh-Taylor instability and the pairing process.

The in-plane magnetic field reduces the magnitude of RT growth rate for all wavelengths and fully stabilizes it for the small wavelength $\lambda < 1$.

Since the in-plane magnetic field partially inhibits the RT instability, the energy cascade process corresponding to the vortex pairing can proceed.

At the same time macroscopic structures inside the vortices with typical dimension greater than unity, because of the stabilization of the small wavelengths, are created by the RT instability.

The complete disruption that takes place in the unmagnetized case does not occur and no filamentary mixing layer forms[8]. In the unmagnetized case $\Delta n = 0.8$ is large enough to lead to the disruption of the pairing process and of the vortices themselves. Here the stabilizing effect of the magnetic tension prevents the vortex disruption and preserves the pairing process.

---

[8]M. Faganello *et al.*, Phys. Rev. Lett. **100**, 015001 (2008).

Rayleigh-Taylor induced reconnection.

During the vortex growth the high and the low density plasma regions roll up carrying and stretching the in-plane magnetic field lines (see Fig. 6) and thus causing the formation of inversion regions where reconnection can develop. When and where magnetic reconnection takes place depends on the competition between the vortex pairing and the development of the secondary RT instability.

In the case of a moderate initial density jump $\Delta n = 0.3$, reconnection occurs only during the pairing process and acts mainly in the region between the two merging vortices, see Fig. 4, first row, central frame.
This evolution is similar to that which occurs in the case of a uniform density configuration[9].

---

[9]M. Faganello *et al.*, Phys. Rev. Lett. **101**, 105001 (2008), Phys. Rev. Lett. **101**, 175003 (2008), New J. Phys. **11**, 063008 (2009).

On the contrary, when the initial density jump is larger, $\Delta n = 0.8$, the RT instability develops inside the vortices and perturbs the structure of each vortex. As the deformations of the vortex arms driven by the RT instability grow, the current layers inside each arm are compressed forcing the the development of the reconnection process.

For large density jumps magnetic field line reconnection occurs before the pairing process and inside each vortex, not between vortices. This reconnection process is thus induced by the local RT instability in a way analogous to the case of reconnection induced inside each vortex by the KH instability[10] and occurs on the fast time scale of the RT instability.

The correlation between the RT and reconnection can be seen qualitatively and quantitatively. E.g., he typical time of the induced reconnection can then be estimated as $1/\gamma_{rec} \sim 5$, which is consistent with the growth time of the RT instability.

---

[10]Z.X. Liu *et al.*, Geophys. Res. Lett. **15**, 752 (1988), Q. Chen *et al.*, J. Geophys. Res. **102**, 151 (1997), D.A. Knoll *et al.*, Phys. Rev. Lett. **88**, 215003 (2002), F. Califano *et al.*, Nonlin. Processes Geophys. **16**, 1 (2009).
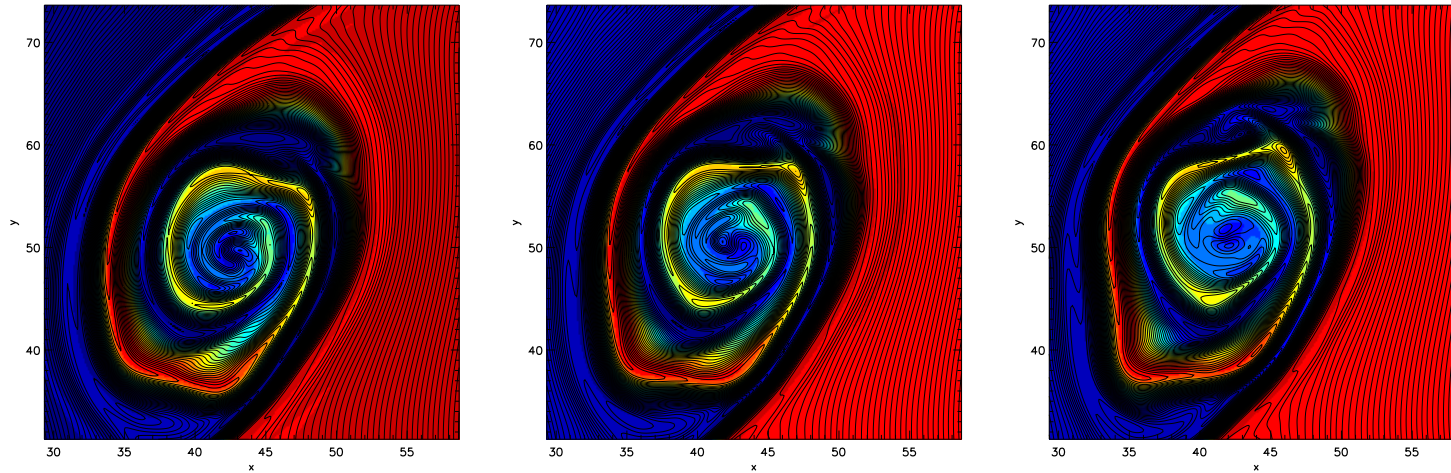
Figure 7: A hydrodynamic perturbation around $x = 44$ and $y = 60$ induces magnetic reconnection. The growing perturbation is shown for $\Delta n = 0.8$ at $t = 364$ (left frame), $t = 369$ (central frame) and at $t = 374$ (right frame).

Conclusions

The nonlinear dynamics of a fluid 2D plasma configuration with a sheared velocity field has been discussed with the help of numerical simulation results.

Main focus: the effects of the density inhomogeneity and of the in-plane magnetic field on
1) the competition between the Kelvin-Helmholtz primary instability, with its nonlinear evolution characterized by the vortex pairing process,
2) the onset of hydrodynamic secondary instabilities, such as the Rayleigh Taylor instability (driven by the vortex rotation and the density inhomogeneity),
3) the onset of magnetic field line reconnection (driven by the stretching of the frozen-in in-plane magnetic field due to the differential plasma motion caused by the Kelvin-Helmholtz and the Rayleigh Taylor instabilities).

The density inhomogeneity controls, through the development of the Rayleigh Taylor instability, the amount of disruption of the pairing vortices before they merge into a single structure.

The role of the in-plane magnetic field is multi faceted as it leads to the formation of small scale magnetic islands through the development of induced magnetic reconnection but at the same time preserves the global coherence of the vortex merging process and suppresses small wavelength perturbations.

When and where magnetic reconnection takes place depends on the competition between the vortex pairing and the development of the secondary RT instability and it is thus itself controlled by the density inhomogeneity.

Model description. Details

We consider a 2D description of the system, with the inhomogeneity direction along x, the periodic direction along y, and z an ignorable coordinate.

We adopt a two-fluid, quasineutral plasma model. The electric field $\mathbf{E}$ is calculated by means of the following generalized Ohm's law[11] ($\mathbf{u_e}$ electron velocity, $\mathbf{u_i}$ ion velocity, $\mathbf{j} = ne(\mathbf{u_i} - \mathbf{u_e})$)

$$\left(1 - d_e^2\,\nabla^2\right)\mathbf{E} = -\mathbf{u}_i \times \mathbf{B} + \frac{1}{n}\,\mathbf{j} \times \mathbf{B} - \frac{1}{n}\nabla P_e\,,$$

where we use the following normalization quantities: $\bar{u} = u_A$; $\bar{\omega} = \Omega_i$; $\bar{l} = u_A/\Omega_i = c/\omega_i = d_i$; $\bar{n}$; $\bar{P}_{p/e} = \bar{n}m_i u_A^2$; $\bar{E} = m_i u_A \Omega_i/e$; $\bar{B} = m_i c\Omega_i/e.$

● In the simulations, the **boundary conditions**, the symmetry of the initial configuration and the **simulation box size** have been optimized in order not to affect the evolution of the system artificially.

---

[11]see e.g., F. Valentini *et al.*, J.Comp. Phys. **225**, 753 (2007)

In detail: 2+1/2 dimensional code, i.e. fields are three dimensional but they depend on the two spatial variables x, y only (and on time).

The dimensions of the simulation box are $L_x = 90$ and $L_y = 30\pi$. The box length in the periodic y-direction has been chosen in order to have two or three vortices ($L_y \sim 2\lambda_{fgm}$).

We choose periodic boundary conditions in the y-direction. Boundary conditions along the inhomogeneous x-direction: we assume that at the boundaries, far from the central region where scale lengths of the order of d_i form, the system is described by the MHD model.

The set of MHD equations is of the hyperbolic type for which it is possible to define the projected characteristic curves in the x direction[12]. Thus we can control the sonic and alfvénic perturbations generated by the dynamics induced by the KH instability entering and leaving the simulation domain and, as a consequence, build up transparent boundary conditions[13].

In the code we employ a third-order Adams-Bashforth method for the temporal advancement. In order to calculate the spatial derivatives the code makes use of sixth-order Compact Finite Difference schemes[14] in the x-direction and Fast Fourier Transforms in the periodic y-direction.

---

[12]S. Landi et al., *A. J.*, 624, 392-401 (2005); K. W. Thompson, *J. Comput. Phys.*, 68, 1 (1987).
[13]M. Faganello et al., *NPJ*, 11, 06338 (2009)
[14]S. K. Lele, *J. Comput. Phys.*, 103, 16 (1992).

The model equations written explicitly are:

$$\frac{\partial n}{\partial t} + \nabla \cdot (n\mathbf{U}) = 0 \tag{1}$$

$$\frac{\partial (n\mathbf{U})}{\partial t} = -\nabla \cdot \left[\frac{n}{1+d_e^2}(\mathbf{u}_i\mathbf{u}_i + d_e^2\mathbf{u}_e\mathbf{u}_e) + \frac{1}{1+d_e^2}\left(P_e + P_i + \frac{B^2}{2} - \mathbf{BB} \right) \right] \tag{2}$$

$$(1 - d_e^2\nabla^2)\mathbf{E} = -\mathbf{u}_e \times \mathbf{B} - d_e^2\left\{ \mathbf{u_i} \times \mathbf{B} + \frac{1}{n}\nabla \cdot [n(\mathbf{u_i}\mathbf{u_i} - \mathbf{u_e}\mathbf{u_e})] \right\} \tag{3}$$

$$\mathbf{u_e} = \mathbf{U} - \frac{1}{1+d_e^2}\frac{\mathbf{j}}{n} \ , \ \mathbf{u}_i = \mathbf{U} + \frac{d_e^2}{1+d_e^2}\frac{\mathbf{j}}{n} \ , \ \mathbf{U} = \frac{\mathbf{u}_i + d_e^2\mathbf{u}_e}{1+d_e^2} \tag{4}$$

$$\nabla \times \mathbf{E} = -\frac{\partial \mathbf{B}}{\partial t} \ , \ \nabla \times \mathbf{B} = \mathbf{j}. \tag{5}$$

The values of the parameters that are kept fixed in the simulations are

$$L_{eq} = 3, \ \Delta U = 1.0, \ T_e = T_i = 0.5, \ n_0 = 1, \tag{6}$$

$$B_0 = 1, \ B_{0y} = 0.02, \ M_s = 1, \ m_p/m_e = 64.$$